Laser-Induced Porous Graphene Sponge for Oil Absorption

Katherine Atwater, Eric Bailey, Allen Chang,
Griffin Godbey, John Mecham, Amine Oueslati

ENMA490 Capstone Design Course

Abstract

Over the past 37 years, more than 13 large-scale oil spills have damaged animals' habitats, the environment's ecosystems, the world's economy, and human-life as a whole. Current oil sponge and oil absorbent technologies are plagued by significant environmental impact, high cost, complex and resource intensive manufacturing, and the lack of oil-water selectivity. Recently, a comparatively inexpensive and scalable fabrication technique has emerged where a polyimide film is converted to porous graphene through radiation by an infrared laser [1]. This research aims to design a new oil sponge from this laser-induced graphene that has high capacity, mechanical stability, excellent selectivity, and reusability. Atomistic modelling in VASP confirmed energetically favorable alkane sorption on porous graphene. Molecular dynamics, using the AIREBO potential, was used to study the sorption of several octane molecules, representative of oil, on porous graphene. To design the sponge to maximize fluid flow and uptake properties, a finite element approach using Darcy's Law was used to simulate the flow of oil through porous graphene. In these simulations, it was found that the ideal design includes ventilation in the polyimide substrate so the oil can flow into the bounded system. Prototypes were obtained and used for experimentation. From the atomistic simulation and experimental data, we have shown that despite the porous graphene oil sponge's low than expected performance, there is promise in increasing sorption via the ventilation process.

Motivation

Graphene has been exploited for its unique physical, chemical, electrical, and mechanical properties by applying it to various applications. Through designing and manipulating the synthesis procedure, a three dimensional (3D) network of pores can be formed in the carbon network of a graphene sheet. This "defective" structure makes porous graphene appealing to even more applications ranging from filters to energy storage devices. Conventional porous graphene processing techniques are not considered scalable (and therefore not commercially feasible) due to high processing temperatures and/or multiple, lengthy, and complex synthesis steps. Recently, a scalable pulsed laser synthesis technique was demonstrated to make porous graphene from Kapton polyimide (PI) [1]. As a result, there is now an opportunity to implement laser-induced porous graphene (LIG) in mass quantities.

The oleophilic, hydrophobic, and mechanical properties of LIG make it an appealing candidate material for oil sponges (i.e. devices used to remove oil from water). Large scale oil contamination of water occurs infrequently, but when it does occur, the impact is devastating. Oil contamination imposes significant threats and damage to human health, ecosystems, the economy, and more [2]. Millions of gallons of oil spill during each catastrophe, destroying habitats and polluting ecosystems. Recently, carbon-based oil sponges have been shown to have exceptional oil uptake properties, but these technologies have not been extensively investigated. The successful design of a LIG oil sponge would greatly impact the recovery from oil spills due to its high oil absorbance and easy reclamation of the absorbed oil.

Current technology does not allow for effective oil removal. Polypropylene and polyurethane, 2 previously used technologies, can only soak up 20 to 30 grams of oil and water per gram of polymer. The non-selectivity of these polymers decreases the efficiency of the materials as oil sponges. Graphene is

oleophilic and hydrophobic making it an ideal oil sponge material that, through further processing, can be made even more hydrophobic [3].

The development of a scalable fabrication technique for porous graphene coupled with a device designed with optimal pore size, pore density, and number of sheets may be able to address current challenges in cleaning up oil spills and prevent future catastrophes.

Material Science & Engineering Aspects

This project has many Material Science and Engineering aspects that build off of concepts in kinetics, thermodynamics, and computational materials science. First and foremost, our project is based on graphene, an emerging material used in a wide array of applications and whose fundamental working principles are still being explored. Graphene is well known for its unique properties, but its marketable applications are still few and far between. As a team, we are exploring the potential to use LIG as a marketable oil sponge technology.

In addition, we also draw upon kinetics and thermodynamics in our analysis and understanding of alkane-graphene interactions. Determination of the interaction energies, based on Equation 1, between different systems (alkane-alkane, alkane-graphene, alkane-water, water-water, water-graphene, graphene-graphene) allowed us to confidently hypothesize that the alkane-graphene interactions would be most favorable.

$$\Delta E_{int} = E(A,B) - (E(A) + E(B)) \tag{1}$$

We also determined the plausibility of chemisorption and physisorption occurrences within our simulation. Knowing the chemistry, Figure 1, and energetics of our graphene and alkanes, we determined that the kinetics of physisorption were more feasible than the thermodynamics and chemistry of chemisorption (i.e. the adhesion of alkanes to graphene is not a chemical bonding phenomenon). We also use basic polymer engineering concepts to reinforce the notion that n-alkanes, which are nonpolar in structure, will prefer to wet the nonpolar graphene matrix.

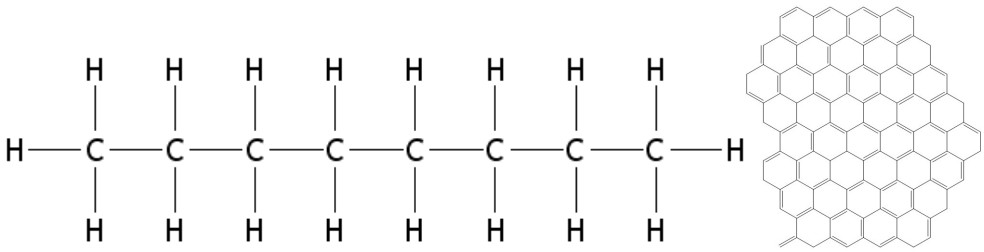

Figure 1. Left: n-Octane and Right: Graphene are both nonpolar molecules as demonstrated by the lack of charged or partially charged side groups.

Furthermore, the bulk of our project was modeled using computational materials science, a field of study that draws on principles from solid state physics, kinetics, and thermodynamics. In order to run our simulations, we had to find, select, and implement pair potentials based on modified versions of the

basic Lennard-Jones pair potential, Equation 2. The process of modeling graphene and n-alkanes required previous knowledge of crystal structure, polymer behavior, and atomic interaction potentials.

$$V_{LJ} = 4\varepsilon \left[\left(\frac{\sigma}{r} \right)^{12} - \left(\frac{\sigma}{r} \right)^{6} \right] = \varepsilon \left[\left(\frac{r_m}{r} \right)^{12} - 2 \left(\frac{r_m}{r} \right)^{6} \right], \quad (2)$$

Previous Work

Laser-induced graphene

The Tour group at Rice University developed a method for creating porous graphene from PI film by laser irradiation [1]. By ablating the PI film, all bonds that are not carbon-carbon bonds were broken leaving porous graphene behind on the non-irradiated PI substrate. The group used this method for the purpose of creating microsupercapacitors and other energy storages devices that would benefit by the highly controllable geometry allowed by laser ablation. It was found that different laser powers changed graphene film thickness, porosity, and pore size, suggesting a method for tunable porous graphene. Samples created with a 3.6 W CO_2 IR laser were found to have pore sizes with a majority in the 2.36 nm-3.68 nm diameter range and a specific surface area of 342 m^2/g [1]. With such high porosity, ease of manufacture, and adjustable physical properties, we believe this material could be pioneered to be an oil sponge.

Comparison to existing technologies for oil removal

Current technology does not allow for effective oil removal. The most commonly used polymer for oil absorption is styrenebutadiene rubber (SBR) [4]. SBR is classified as an oil solidifier and does not selectively absorb oil [5]. Recently, researchers have moved towards carbon nanotubes (CNTs) and graphene as oleophilic sponges. Additional processes can make these materials more hydrophobic allowing more ideal oil absorption [3].

Such technologies would be highly sought by offshore oil companies to combat disasters. Not only will the graphene sponge be more efficient at removing oil, oil companies can reclaim their lost oil by compressing the sponge after saturation. Millions of gallons of oil are spilled per year [3] and the possibility that 80% of this oil can be reclaimed is significant, especially in a time where the reserves of oil are becoming increasingly harder to extract.

Polyurethane has also been under investigation for oil sponge applications. These sponges can absorb about 20 grams of oil per gram of sponge and they are relatively inexpensive. It is important to note that these sponges are not hydrophobic naturally, but they can be treated with nanoparticles to introduce hydrophobicity and increase oil sorption. These additional processing steps are expensive and difficult to estimate in price and will not be considered in our following calculations. Polyurethane sponges, regardless of surface treatment, still experience rapid deterioration with cycling [6]. All-Spec.com sells foam polyurethane 24” x 36” x ¼” sheets, weighing approximately 0.3 lbs, at the low cost of $20.10.

In 2012, the Ajayan group at Rice University developed an oil sponge made from carbon nanotubes. The sponge is 99% porous with good mechanical and electrical properties. These sponges will be popular among oil companies and environmentalist due to their reusability and hydrophobic behavior; however, these sponges are very expensive because they are made with all CNTs. The cost of CNT

powders from Sigma-Aldrich is $100 per gram. The catalytic chemical vapor deposition (CCVD) is what drives up the price of these materials. The Ajayan group reported the CNT sponges can absorb 80 grams of oil per gram of CNT sponge and the average density of their sponge to be 20 mg/cm^3 [7].

The Tour group at Rice University produced their LIG from Kapton PI film which is trademarked by the chemical company, Dupont. To purchase a 0.0003" x 24" x 120" film of PI, approximately 20.1 g, costs $20.74. LIG has never been analyzed for oil absorption in the past; however, other porous graphene sponges have been reported to absorb 80 grams of oil per gram of graphene. Graphene is a promising material due to its natural oleophilic and hydrophobic properties.

Cost analysis of LIG compared to existing technologies

The successful design of the graphene oil sponge would greatly impact the recovery from oil spills due to its high oil absorbance and easy reclamation of the absorbed oil. While oil spills are not frequent, their effect on the environment is substantial through the destruction of local ecosystems [2]. In this study, we compare a theoretical LIG oil sponges to existing sponge technologies.

The most critical problem with polyurethane is that natural polyurethane is not hydrophobic, meaning it will absorb oil and water alike. Other than that, the absorption is very low and the polymer is not very dense. Assuming polyurethane sponge material absorbs 20 grams of oil per gram of sponge, polyurethane cost $0.00739 per gram of oil and water absorbed per use. Calculating the density of the polyurethane block from All-Spec.com came out to be .0384 g/cm^3. The polyurethane sponge is calculated to hold .768 grams of oil per cm^3.

The main issue with CNT sponges is their price. We estimate CNT sponges are so expensive that the price of absorbing oil is $1.3 per gram of oil per use. Assuming that each gram of CNT absorbs exactly its theoretical oil absorption, we see the CNT sponges absorb 1.6 grams of oil per cm^3.

Graphite can be considered a non-porous variant of LIG, due to their identical interlayer spacing of 3.4 Å. The known density of graphite is 2.26 g/cm^3 and from the BET results in figure S7 from Lin, J. et. al. [1] we calculated the LIG to be 85.5% porous. This gives the LIG sponge a theoretical density of 328 mg/cm^3. Porous graphene from research has had moderate density with a high absorption ratio meaning the spatial efficiency of absorbing oil will be high, 26.24 gram of oil per cm^3 theoretically. Assuming we can convert half of the PI into graphene, we would get 7.13 g of graphene taking into consideration that oxygen and nitrogen are burned off in the lasing process, its cost of production is second compared to polyurethane at $0.0364 per gram of oil absorbed per use.

LIG shows great potential as an oil sponge as far as cost and spatial efficiency are concerned. It fully and selectively extracts crude oil from water despite a moderate cost increase compared to polyurethane sponges and it collects oil with a greater spatial efficiency than polyurethane. LIG sponges are much cheaper than CNT sponges and they have better spatial efficiency during collection of oil.

BP Deepwater Horizon Oil Spill Alternate Response Analysis

During the BP Deepwater Horizon Oil Spill in 2010, 210 million gallons of oil spilled from an offshore oil rig explosion. The cleanup effort took many years and environmental effects can still be seen today. Over $14 billion and 70 million personnel hours were spent towards cleaning up the lost oil [8].

The primary method to dispose of the oil was the use of the dispersant Corexit 9500 which has been criticized for being harmful to the environment. Corexit 9500 breaks down large crude oil components into small pieces, making it easier for microbes in the ocean to break down the oil. Oil is not recollected once Corexit is used [8]. The current price of Corexit 9500 from cleancaribbean.org is

$17,078 per 330 gallon container. BP used approximately 1.84 million gallons (21.1 m^3) of dispersant to clean up the Gulf of Mexico, which cost over $1 billion. There is no direct mention of how many gallons of oil the 1.84 million gallons of dispersant were affected, so for the simplicity of this case study, it will be assumed that 1.84 million gallons of dispersant dispersed all 210 million gallons of crude oil. Corexit selectively targets crude oil and is not reusable after the first use.

Reviewing some of the previously calculated information, we can see that if BP used all polyurethane sponges, it would cost them approximately $513 million dollars and require 902,000 m^3 of shipping space to the site of the oil spill. Polyurethane is not selective meaning it will absorb water and oil alike making a very inefficient oil absorbing material. This method of oil removal is almost half as expensive of the Corexit option but requires significantly more volume of storage, making the use of polyurethane sponges a viable option for oil clean up only due to the inexpensive nature of the materials.

CNT sponges have also been studied as potential oil sponges. If CNT sponges were to replace the Corexit used during the Deepwater Horizon spill, BP could have potentially recovered some of their lost oil for further processing. CNTs are far more expensive than the current technology. The advantages of CNTs over dispersants are environmental stewardship of fully removing spilled oil and the easy method used to remove the oil from the sponge. CNT sponges are reusable; however, their reusability has not been fully explored. Suppose BP could reuse a CNT sponge ten times for the 2010 oil spill, they would still end up paying $91.3 billion dollars in material costs and require 43,500 m^3 of transportation space. While CNTs are oil selective, reusable, and allow oil recovery, their expensive cost makes them hard to justify as a viable oil sponge material.

LIG, like CNTs, have sponge-like characteristics, which means spilled oil could be reclaimed. LIG is more expensive than Corexit, but LIG is reusable at least up to 10 times with greater than 99% maximum capacity [9]. While previously explored, LIG is a rather expensive material, its cost decreases vastly when considering reusability and recovered oil. If BP were to use LIG single use to clean up 210 million gallons of oil, it would cost $25.2 billion in materials, but if they reuse each LIG sponge ten times during the cleanup effort, that material cost decreases to $2.52 billion dollars. Additionally, if BP were able to reclaim 80% of the lost oil at the cost of $60 per barrel, BP would see a net loss of only $2.22 billion. LIG is more beneficial to the ecosystem than Corexit because it immediately removes the oil from the environment rather than breaking it down into small pieces and waiting for natural decomposition. While polyurethane absorbs water and crude oil alike, LIG selectively absorbs nonpolar fluids, thus saving time on oil removal. The high density of LIG makes shipping costs cheaper. To clean up all 210 million gallons of crude oil, BP would only need 2,640 m^3 of ship space. While this material loss is still more than the material loss of using Corexit 9500, this option is still viable because the LIG sponges should still be reusable after 10 cycles saving BP money on future spill cleanup efforts.

Table 1: BP Deepwater Horizon disaster response comparison of current technology (Corexit 9500 dispersant), polyurethane sponges, CNT sponges, and LIG sponges. Corexit 9500 did not disperse all 210 million gallons of crude oil, true value unknown. CNT sponges and LIG sponges reused 10 times each.

Method	Cost (Billions of dollars)	Volume (m^3)	Selectivity	Recovery	Environmentally Safe
Corexit 9500	~$1	~21.1	Yes	No	No
Polyurethane	$0.513	~902,000	No	No	Yes
CNT sponge	$91.3	~43,500	Yes	Yes	Yes
LIG sponge	$2.52	~2,640	Yes	Yes	Yes

Table 1 summarizes the findings of our group's theorizing of the impact of the use of LIG in place of Corexit 9500. We believe that LIG is the best alternative of CNT sponges and polyurethane sponges due to its relatively low cost, environmentally friendly oil removal, high density of oil adsorption, and promise of oil recovery. For these reasons, we believe LIG has potential to be a great oil sponge.

Design Goals

Our goal for this project is to determine the influence of porosity on oil sorption and to test the viability of utilizing LIG as an oil sponge. We aim to model the sorption of alkanes present in crude oil using both atomistic and fluids modeling. From these models, we aim to determine the effect of porosity and pore size on maximum oil sorption and the optimal design for a LIG oil sponge. We will also experiment with prototypes to support the validity of our models.

Previous porous graphene sponges are not supported by a substrate and are more difficult to use for recollection after use [9]. Our design includes a porous graphene medium that is attached to a PI film. This not only gives the sponge mechanical support, but also enables it to be potentially attached to a floating substrate to facilitate its recollection. To optimize the design parameters of the LIG we will investigate oil flow and sorption on the macroscale and nanoscale. Matlab will be used to simulate fluid flow and diffusion using Darcy's law and Fick's diffusion law. On the nanoscale, we can make use of VASP and LAMMPS to further understand the interactions between oil molecules and the porous graphene layers. This will allow us to relate pore size and interlayer spacing to oil sorption. This differs from previous modeling of oil sorption by focusing on the porosity of the graphene instead of just surface sorption to a pristine sheet as done in previous works [10]. Using this information, we will be able to ameliorate the manufacturing process of LIG to get it close to its maximum absorbance capacity.

Technical Approach

Atomistic Simulation

We utilize atomistic modeling to understand the atomic interactions between the porous graphene and the alkanes present in crude oil. Before simulating adsorption interactions, we proceeded to understand fundamentals pertinent to our system. We studied energetics between alkane molecules and graphene to verify that graphene would preferentially sorb onto graphene. We also simulated graphene under various conditions (e.g. varied temperature and time scales) to confirm that the graphene would undergo no significant changes (i.e. pore diffusion or catastrophic failure) under our alkane-graphene simulation conditions. We then developed a simulation where a constant pressure solution of alkane sits above 2 sheets of graphene, the top of which contained a variable sized pore. Figure 2a shows the schematic view of the simulation where the x and y axes were periodic, allowing the graphene to act as an infinitely long sheet. To prevent atoms from leaving the confined box we applied a boundary forces on the z axis. Figure 2b is the corresponding view of the simulation.

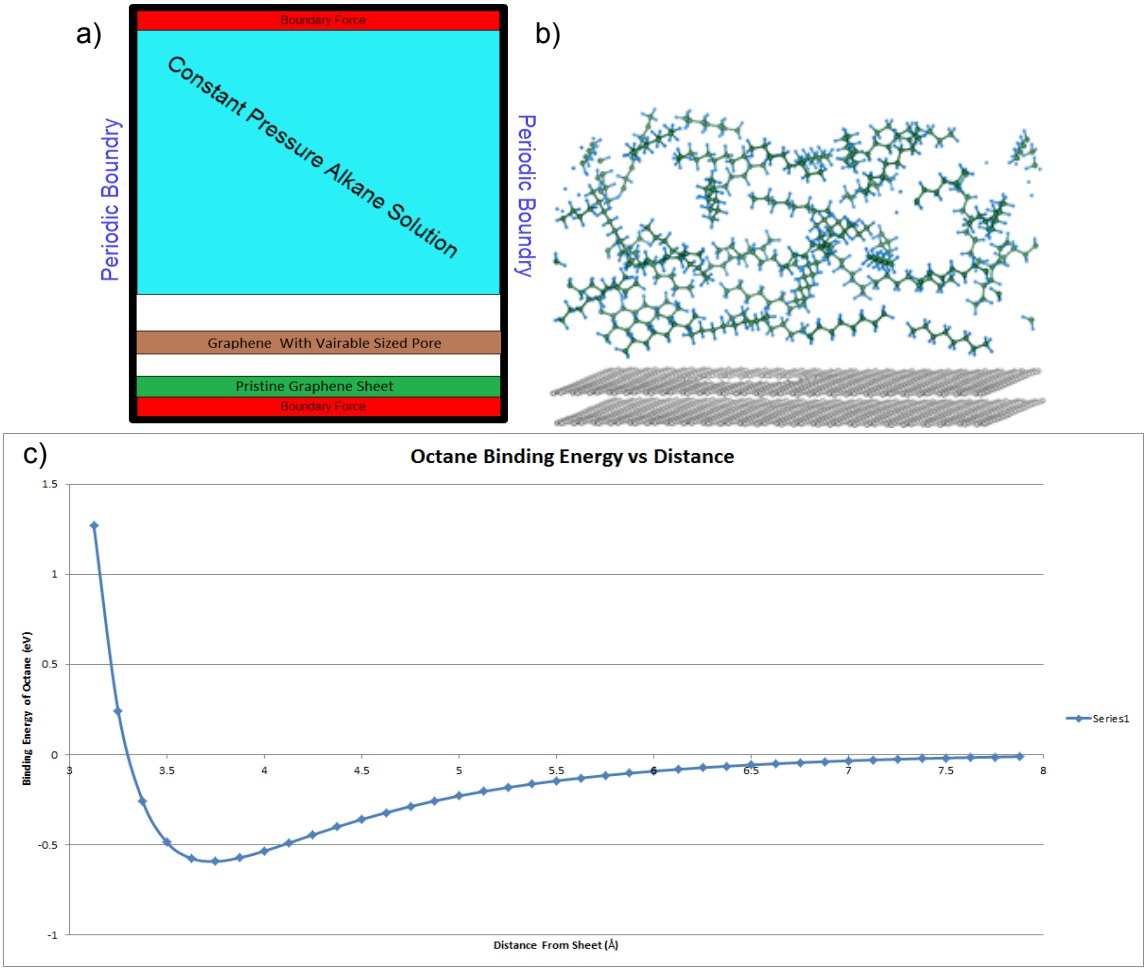

Figure 2. a) Simulation schematic. b) Simulation snapshot. c) Octane binding energy vs. distance from sheet.

To measure the number of physisorbed molecules we examined the energy between each alkane and each corresponding sheet. If the binding energy was found to be less than -.55eV, then we counted the molecule as being adsorbed to the sheet. We arrived at this energy by choosing a value at the bottom of the potential well; however, this value is very conservative value. When we simulated an octane solution, we found that the average binding energy of octane in solution was ~ -0.25eV hence, a binding value lower -0.25eV should indicate that the octane is more favorable near the sheet. Lastly we ran a simulation where there was no pristine sheet below graphene sheet with the pore. We found that even small pores (as small as 4 angstroms) allowed for diffusion of alkanes to the back side of the sheet.

Fluid Simulation

In addition to atomistic modeling, considerations of fluid flow mechanics were suggested by Dr. Chandra Thamire. In our simulation of fluid flow and capillary effects, we aim to understand and utilize Darcy's Law [11], Equation 3, where J is the flux, κ is the intrinsic permeability of the medium, ∇p is the pressure gradient, and μ is the viscosity.

$$J = \frac{-\kappa}{\mu}\nabla p \qquad (3)$$

Synthesis

We produced a number of graphical models to investigate the effects of pore size on relative oil absorbency of porous graphene. These graphs will be used to approximate the optimal pore size of a graphene sample that would need to be produced to obtain relatively high oil sorption properties and understand the sorption behaviors of octane on porous graphene. We also completed a material cost analysis of our graphene sponge against existing sponge technologies.

Measurements

In order to determine the sorption capacity of our graphene sponge, we measured the mass of our entire sponge device before and after sorption, as well as the PI substrate without the graphene. These measurements allowed us to calculate the mass of the oil sorbed into the graphene, which, in turn, led us to the grams of oil sorbed per gram of graphene. Grams oil sorbed per gram of graphene sponge is demonstrated in Equation 4 below:

$$\frac{Grams\ Oil}{Grams\ Graphene} = \frac{(mass_{final} - mass_{initial})_{sponge}}{(mass_{initial})_{sponge} - mass_{substrate}} \qquad (4)$$

Using our experimental data on sorption capacity and the pore distributions from Lin, J. et al [1], we were able to compare the LIG samples to the theoretical sorption model. In order to obtain these results, we followed the experimental procedure listed below:

Experimental Procedure for Measuring Octane Absorption of Graphene

1. Weigh pristine PI film on microbalance
2. Test PI Oil Sorption
    a. Place sample in dish of octane for one minute
    b. Weigh sample on microbalance
    c. Calculate mass lost or gained to determine octane effects on PI
3. Weigh graphene sponge samples on microbalance
4. Test Graphene Sponge Oil Sorption
    a. Place sample vertically in dish of octane, partially submerged, for one minute
    b. Weigh sample on microbalance
    c. Repeat step a and b, increasing the time of submersion by one minute
    d. Submerge full sample in oil until maximum sorption is reached
    e. Weigh sample on microbalance
5. Remove graphene/oil from PI substrate through exfoliation
6. Weigh exfoliated sample on microbalance to obtain PI substrate mass
7. Subtract PI substrate mass to determine oil absorption per mass graphene
8. Plot curve for oil mass vs time to determine absorption capacity over time
9. Calculate absorption rate via oil mass absorbed per second
10. Calculate maximum sorption capacity of sponge

Prototype

The prototypes for this project were provided by the James M. Tour group at Rice University. Three pieces of PI each with 2.4 cm^2 areas, 25 um thick, laser-induced graphene sections, represented in Figure 3, with known pore sizes and distribution were used for experimental testing. Lin et. al documented the sample fabrication procedures along with the material specifications [1]. A 3.6 W CO_2 laser irradiating the sample at 14 μs pulses was used to ablate the PI, forming LIG. This simple fabrication procedure is both appealing and integral to the future marketability of porous graphene oil sponges. To test our hypothesis we utilized 99% anhydrous n-octane and a microbalance with a calculated accuracy of 0.001 ± 0.01 mg. We measured both maximum sorption of the prototype as well as time dependency of adsorption to test our hypothesis.

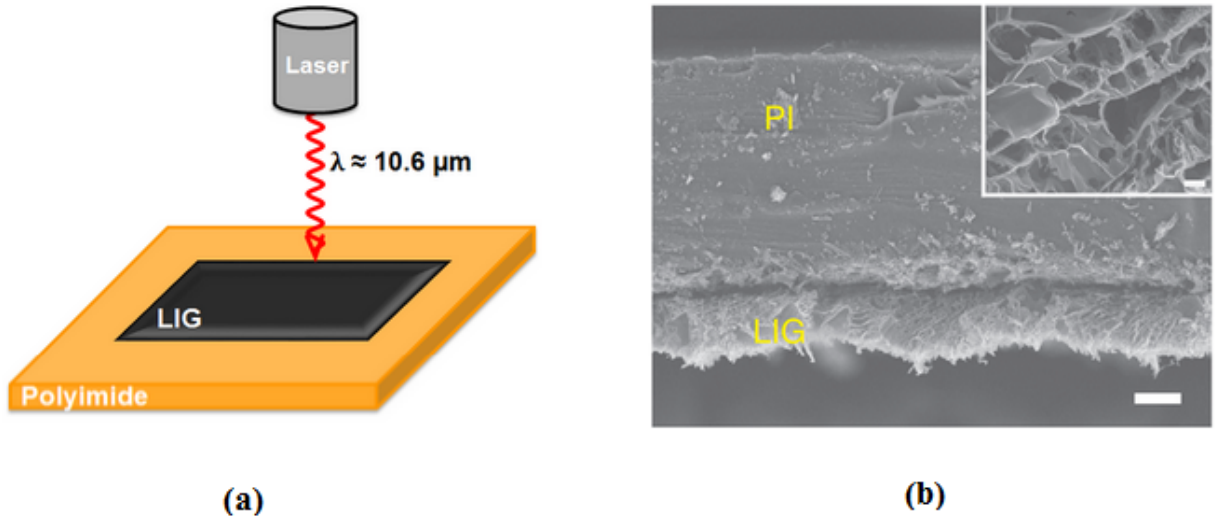

Figure 3. (a) Schematic of sample fabrication. Laser-induced graphene, black, is being ablated from PI, yellow, using a CO_2, 3.6 W, 10.6 μm laser. (b) Scanning electron microscope image of LIG on a PI substrate using a 3.6W CO_2 laser; scale bar, 20 μm. Inset scale bar, 1 μm. [1]

Ethics & Environmental Impact

The purpose of this design is to create a graphene sponge that can clean up oil during an oil spill more cost efficiently than currently existing polymer sponges and be able to recover some of this oil from the sponge after removal from the ecosystem. As mentioned before, SBR and polyurethane are commonly used polymer oil sponges. Unlike graphene, SBR and polyurethane are synthetic polymers whose monomers have been known to be toxic, environmentally unfriendly, and not easily degradable. Styrene, polyols, and diisocyanates used to fabricate oil sponges exhibit many undesirable qualities that graphene could easily alleviate. As a naturally occurring material, graphene is much easier to degrade after use. Some research has been concentrated on synthesizing "green" monomer replacements for polyols and diisocyanates; however, these efforts have not been applied to oil sponge technologies.

The fabrication of these graphene sheets requires large amounts of PI and a CO_2 laser. PI is commonly used and does not have many harmful byproducts of production. CO_2 IR lasers are very common and are relatively inexpensive [12]. CO_2 lasers have a lower cost per watt than all other types of lasers. While only 10% of the laser's input power generates laser energy, this is still a relatively small input energy compared to the oil that will be recovered. Thus, the energy and materials consumed to create LIG do not outweigh the benefits of its creation.

By using graphene as an oil sponge instead of polyurethane, there should be a greater oil absorption (80g of oil per 1g of porous graphene) than the current technology with the possibility of high oil recovery. Polyurethane absorbs oil, but is less effective in recovery than the graphene sponge we hope to design [6]. In this fashion, graphene is not only efficient, but also reusable; therefore, a graphene oil sponge does not have to be processed as waste after a spill has been cleaned, but can instead be reused during the next clean-up effort.

To the extent of our knowledge, the graphene oil sponge device is benign to society and the environment. The consequences of developing such a device should have little to no

manifestation as a harmful or manipulative tool. We have developed an environmentally friendly device that should face very few ethical challenges.

Intellectual Merit

This study will help increase understanding of the effect of pore size, pore density, and number of graphene sheets on the oil uptake properties of porous graphene. To our knowledge, this has not been done either computationally or experimentally. As a result of this project, we hope to design an optimal graphene sponge device for removing oil from water and increase the body of research relating to the sorption properties of porous graphene. In addition, we hope that our findings will provide a foundation and fundamental understanding of this technology for future innovations in this field.

Broader Impacts

The results of this project can be used to increase the marketability of carbon-based oil sponges. Currently, producing porous graphene in mass quantities is not feasible, but extensions of this research can be made to improve future carbon-based oil sponge technologies. Not only will this project propagate graphene sponge technology, but carbon aerogels and carbon nanotube networks may benefit from the understanding of porosity on sorption in carbon-based sponges. There is also potential for these results to impact carbon aerogels in thermal clothing applications. The porous nature of carbon aerogels and the interactions with surrounding media could bring alkanes or other short chain oligomers into contact with the aerogel [13].

Results & Discussion

VASP and Energy Minimization Results

Confirmation of alkane positioning on graphene sheet

In order to better understand the preferable orientation of an alkane on a pristine graphene sheet, we completed an energy minimization with configurations of graphene and octane at angles of -50^{o} to 50^{o} degrees. The energy minimization allowed us to determine the local minimum at these angles.

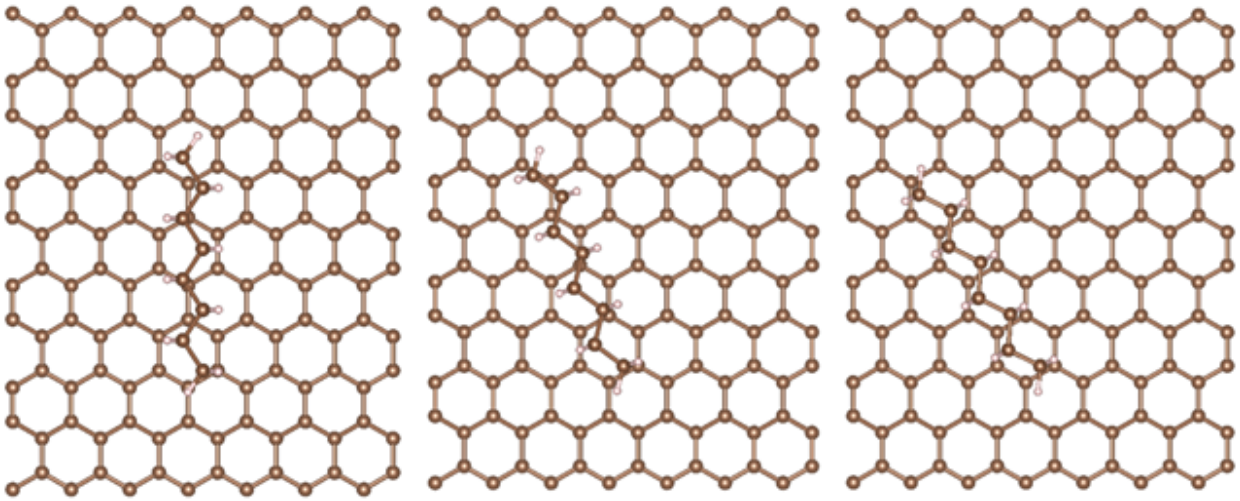

(a) **(b)** **(c)**

Figure 4. *Orientations of octane on graphene at the reference orientation* ***(a)*** *0^{0}, and* ***(b)*** *-20^{0}, and* ***(c)*** *-30^{0} which correspond to the lowest and highest energy systems tested respectively.*

Analyzing the configurations of the lowest and highest final energies in Figure 4, we conclude that the octane preferentially organizes on the graphene sheet so that its carbons are in the space between two graphene carbons, Figure 4b. This configuration was also found to be the most energetically favorable configuration of an alkane and graphene by Kamiya et al. [14], where the alkane preferentially sits on the graphene sheet along the zigzag direction. Our model has minimum energy in the configuration closest to this zigzag direction and thus agrees with the literature.

Alkane binding energy with other alkanes and graphene

We also considered the binding energy between two alkanes versus an alkane and graphene to show that the oil will preferentially bind to the graphene instead of itself. Because octane is one of the most prevalent long chain alkanes in crude oil, we utilized octane in our model. First we determined the minimum energy of an octane molecule in a dilute solution. This returns the energy of just the octane and no other interactions in VASP. We ran a similar model for graphene alone to determine the energy of a graphene sheet. Finally, we ran energy minimizations of octane-graphene and octane-octane systems. We proceeded to calculate the binding energy of every case using Equation 5.

$$Binding\ Energy = E_{system} - E_{molecule\ 1} - E_{molecule\ 2} \qquad (5)$$

Inserting these final energy values into Equation 5, we were able to calculate the binding energy for octane-octane to be -0.0274eV and the binding energy of octane-graphene to be -0.3569eV. The octane-octane energy was calculated utilizing an average of energies for different octane-octane configurations, since the octane molecules in oil will be randomly oriented. Analyzing these results, it is obvious that our model shows octane-graphene as the more energetically favorable system, which agrees with the findings of Kamiya et al. [10], who found the binding energy of octane-graphene to be -0.57eV. We believe that our binding energy value is slightly off from that in the literature due to our octane molecule not being perfectly aligned on the zigzag direction of the graphene sheet, as seen in Figure 1B. Overall, these results verify that graphene will attract crude oil due to a more favorable binding energy and thus our graphene sponge should collect oil.

Molecular Dynamics (MD)

In order to understand the movement of the atoms in our system at nonzero finite temperatures, we conducted Molecular Dynamics. This method has been used to investigate the movement of carbon atoms and pores at elevated temperatures and study the sorption of alkanes on porous graphene.

Vacancy Diffusion in Graphene

In order to determine vacancy movements in graphene, we heated our porous graphene sheets from 0 K to a finite temperature, typically 1000 K. This temperature was chosen to show atomic vibrations, reduce the computation time, and ensure the graphene C-C bonds would not break. Here, we observed atomic vibrations varying in intensities and pores deforming and changing their shape, but no bonds broke and the pore did not move. We also elevated the temperature to 3000 K as done in a similar study by Lee et al. [15] and saw atomic movement. The results of these simulations suggest that vacancy diffusion is most likely to occur at significantly high temperatures. Thus, we are confident that vacancy diffusion in graphene is not an impactful occurrence within the proposed application environment.

Simulation Results

Our atomistic simulations show the following results: 1) oil sorption is independent of pore size, 2) as many as three layers of alkanes are adsorbing to the graphene sheet, and 3) inter-sheet alkanes are energetically unfavorable. Figure 5 depicts the relationship between oil sorption and pore size,

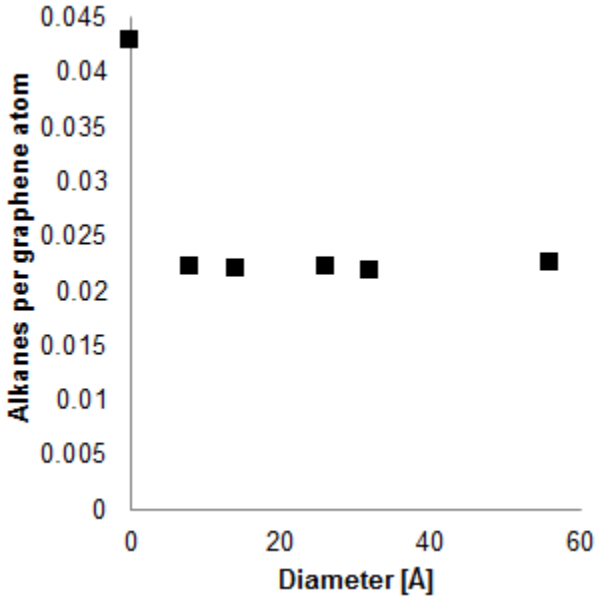

Figure 5. Relating oil sorption to varying pore size.

As seen, the difference in sorbed alkanes per graphene atom is minimal between the various pore sizes. Not accounting for the pristine sheet, the range of data set is ~0.0007 alkanes per graphene atom. The lack of variation here indicates that either LIG behaves differently from our hypothesis or our device is not in its most optimal configuration. Our initial hypothesis was that there would be an almost gaussian distribution of alkanes per graphene atom at varying pore sizes. At small pore sizes, the alkane should not flow through the pore due to physical limitations and at large pore sizes, the alkanes should flow through the hole without any resistance, but there would be less area for surface adsorption. Instead we see that oil sorption seems to be independent of pore size. Thus, we can speculate that there is either only surface adsorption behavior or bulk absorption occurs consistently regardless of pore size. The latter of the two statements is less feasible because, as shown, the pristine sheet has a large sorption compared to porous graphene. The larger sorption in the pristine sheet can be explained by surface adsorption (i.e there is more energetically favorable surface for alkanes to sorb onto in pristine graphene than porous graphene).

Another phenomenon revealed by our simulations is the presence of more than a single monolayer on the porous graphene. By modeling atomic radial distributions, we were able to see characteristic peaks of atomic concentration at set distances from the graphene sheets. In Figure 6, we can see 2 peaks related to the graphene carbons along with multiple smaller peaks which constitute layers of octane.

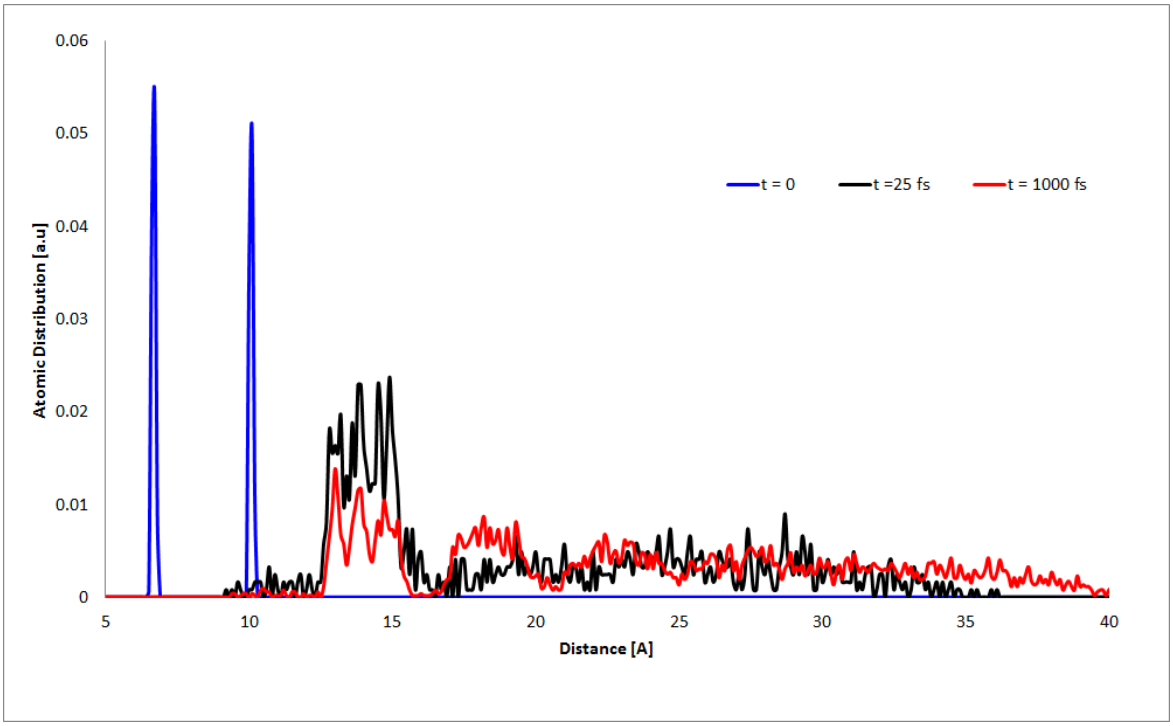

Figure 6. Radial atomic distribution at varying timesteps for pore diameter = 14 A. Formation of layers can be seen by peak formation at longer time steps.

The 2 graphene sheets correspond to the two blue peaks. As expected, the porous graphene top sheet has a slightly lower atomic distribution than the pristine back sheet. The surface monolayer of octane is located at a distance of 13 - 15 A from zero. There is a distinct triple peak which can be attributed to H CC H cross sectional structure of the adsorbed octanes, Figure 7. Further peak formations (~ 18 A and ~23 A for t = 1000 fs) can be attributed to smaller, weaker bonding interactions between alkane and graphene until the separation distance from graphene becomes so large that alkane-alkane binding energies are more favorable than alkane-graphene. This shows promise for future LIG oil sponge research because the oil prefers to interact with the sponge. Once a device is designed for increased fluid flow, the large amount of interacting oil can be easily absorbed.

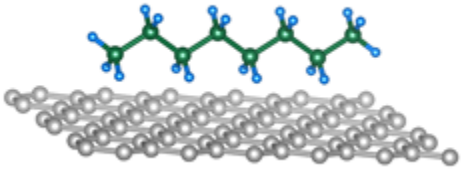

Figure 7. Alkane over graphene sheet with H closest to and furthest from graphene.

The last, and potentially most significant, finding was that inter-sheet alkanes are energetically unfavorable and highly unlikely to occur without external contributions to surpass energy barriers. Figure 8 shows an energy minimized system where an alkane was initialized between 2 graphene sheets along with the graphene-graphene binding energy potential well. The most energetically favorable state requires graphene to bend, a state that has high entropic costs. Despite an interlayer spacing greater than the cross

sectional height of each octane, the carbon-carbon repulsion between graphene and alkane become a source of strain on the graphene sheets.

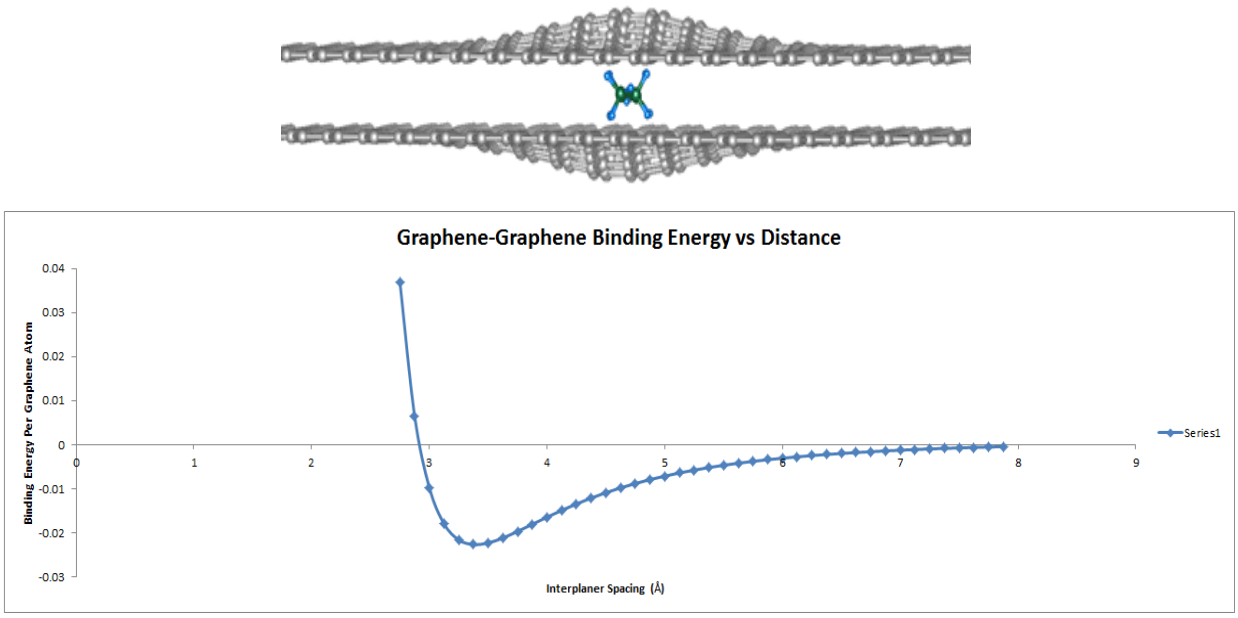

Figure 8. Top: Alkane unfavorably placed between 2 graphene sheets. Bottom: Potential well for graphene-graphene binding energies.

From Figure 8 we can see that each graphene atom that moves away from the alkane has an associated energetic cost. As many atoms move away from their minimized state (i.e. the point of interest moves right to further separations on the potential well), the system becomes less and less favorable. The consequence of this unfavorable configuration is that alkanes flowing through the bulk graphene should be inhibited by the energetic cost of deforming graphene. Thus, we can conclude that, if there exists a high cost for bulk diffusion or flow of octane, our sponge must be experiencing surface adsorption of octanes. This conclusion is supported by the lack of absorption in our experimental testing which will be discussed later.

Fluid Flow Modeling

To understand how the octane will flow through our porous graphene macroscopically, we used a finite element approach. Darcy's law is widely applied to understand fluid flow through porous media and we hope to solve and implement this in MATLAB using experimental and estimated values and parameters [11]. We are attempting to reach this end goal by starting off relatively simple and systematically increasing the complexity. We have represented our system in two dimensions as the cross-section obtained by sectioning the PI-graphene system perpendicularly from the sheets of graphene. Since our system has two axes of symmetry, we chose to model it in two dimensions, specifically with the cross section of our sponge. We began by implementing steady state diffusion, as in Equation FF1.

$$\left(\frac{\partial^2 \Psi}{\partial x^2} + \frac{\partial^2 \Psi}{\partial y^2}\right) = -\omega \qquad \text{(FF1)}$$

Here, ω is dimensionless vorticity defined by $\Omega H / U_0$ where Ω is vorticity (s^{-1}) and Ψ is a dimensionless stream function defined by ψ / HU_0 where ψ is the stream function (m^2/s), H is the height of the sponge (meters) and U_0 is the dimensionless interstitial velocity component. To solve this, we first solved for $\partial^2\Psi/\partial x^2$ in terms of $\Psi(x)$ and $\partial^2\Psi/\partial y^2$ in terms of $\Psi(y)$, then rewrote Equation FF1 using these solutions and solved for $\Psi(x,y)$. Here, $\Psi(x)$ represents the stream function as a function of horizontal position (x) at a constant vertical position (y). To do this, we approximated $\Psi(x+dx)$ and $\Psi(x-dx)$ using Taylor expansions with an infinitesimally small position difference. This process is shown below:

$$\Psi(x+dx) = \Psi(x) + dx\left.\frac{\partial\Psi}{\partial x}\right|_y + \frac{dx^2}{2!}\left.\frac{\partial^2\Psi}{\partial x^2}\right|_y + \frac{dx^3}{3!}\left.\frac{\partial^3\Psi}{\partial x^3}\right|_y + \frac{dx^4}{4!}\left.\frac{\partial^4\Psi}{\partial x^4}\right|_y \cdots \quad \text{(FF2)}$$

$$\Psi(x-dx) = \Psi(x) - dx\left.\frac{\partial\Psi}{\partial x}\right|_y + \frac{dx^2}{2!}\left.\frac{\partial^2\Psi}{\partial x^2}\right|_y - \frac{dx^3}{3!}\left.\frac{\partial^3\Psi}{\partial x^3}\right|_y + \frac{dx^4}{4!}\left.\frac{\partial^4\Psi}{\partial x^4}\right|_y \cdots \quad \text{(FF3)}$$

We can assume that the fourth degree terms (i.e. $\partial^4\Psi/\partial x^4$) and all subsequent terms are small enough and can be ignored. By adding Equation FF2 and FF3, we obtain an equation for $\partial^2\Psi/\partial x^2$ and $\partial^2\Psi/\partial y^2$ as a function of $\Psi(x,y)$ at different spatial locations. The sum of Equations FF2 and FF3 are written below.

$$\Psi(x+dx) + \Psi(x-dx) = 2\Psi(x) + 2\frac{dx^2}{2!}\left.\frac{\partial^2\Psi}{\partial x^2}\right|_y \quad \text{(FF4)}$$

$$\left.\frac{\partial^2\Psi}{\partial x^2}\right|_y = \frac{\Psi(x+dx) + \Psi(x-dx) - 2\Psi(x)}{dx^2} \quad \text{(FF5)}$$

This same equation can be written in terms of $\partial^2\Psi/\partial y^2$, $\Psi(y)$, and dy. These two equations can be written using $\Psi(x,y)$, the spatial specification of the stream function, and combined in Equation FF1. This is shown in Equation FF6. Equation FF7 is obtained by solving Equation FF6 for $\Psi(x,y)$.

$$\frac{\Psi(x+dx,y) + \Psi(x-dx,y) - 2\Psi(x,y)}{dx^2} + \frac{\Psi(x,y+dy) + \Psi(x,y-dy) - 2\Psi(x,y)}{dy^2} = -\omega \quad \text{(FF6)}$$

$$\Psi(x,y) = \left(\frac{2}{dx^2} + \frac{2}{dy^2}\right)^{-1} \cdot \left(\frac{\Psi(x+dx,y) + \Psi(x-dx,y)}{dx^2} + \frac{\Psi(x,y+dy) + \Psi(x,y-dy)}{dy^2} + \omega\right) \quad \text{(FF7)}$$

To implement this equation into our finite element regime, dx and dy were exchanged with finite steps Δx and Δy, respectively. In addition continuous variables x and y were converted to discrete integers i and j, respectively, using $x = i \cdot \Delta x$. Thus, Equation FF7 becomes:

$$\Psi(i,j) = \left(\frac{2}{\Delta x^2} + \frac{2}{\Delta y^2}\right)^{-1} \cdot \left(\frac{\Psi(i+1,j) + \Psi(i-1,j)}{\Delta x^2} + \frac{\Psi(i,j+1) + \Psi(i,j-1)}{\Delta y^2} + \omega\right) \quad \text{(FF8)}$$

To visualize the stream function, we defined our sponge as a 42 point matrix (each point representing a node) and then used Equation FF8 to solve for the stream function at every node. We use

MATLAB's matrix convention (row, column) to define our system. Thus, the top left node is at (1,1) and not (0,0). The model was initialized by defining $\frac{\partial \Psi}{\partial y}$ into the system from the right, left, top and bottom side of the sponge Figure 9.

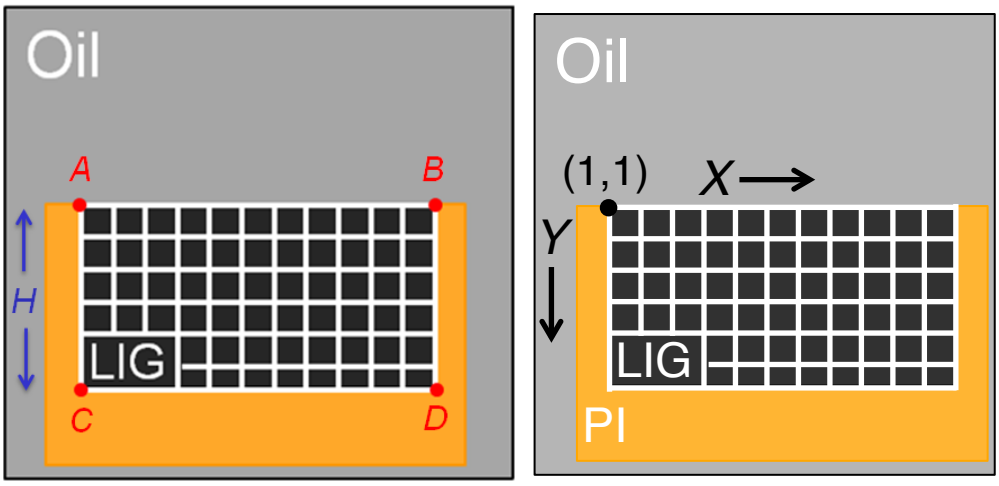

Figure 9. A two dimensional cross-sectional representation of the LIG as a finite grid of nodes.

In the context of our design, the only source of oil is from the open side (top) of the sponge where $\frac{\partial \Psi}{\partial y} \neq 0$. This leads to the four boundary conditions depicted below.

$$\Psi = 0 \quad \text{and} \quad \frac{\partial \Psi}{\partial y} \neq 0 \quad \text{on AB}$$

$$\Psi = 0 \quad \text{and} \quad \frac{\partial \Psi}{\partial x} = 0 \quad \text{on BD and AC}$$

$$\Psi = 0 \quad \text{and} \quad \frac{\partial \Psi}{\partial y} = 0 \quad \text{on CD}$$

Even with these boundary conditions, solving Equation FF1 relies on first solving for the vorticity at a given location. For an arbitrary point (i,j), we want to calculate the vorticity using the local velocities of the four neighboring grid points and the y-direction change in the stream function. In this procedure, vorticity can be defined as such:

$$\omega = \alpha_1 \Psi_{i-1,j-1} + \alpha_2 \Psi_{i,j-1} + \alpha_3 \Psi_{i+1,j-1} + \alpha_4 \Psi_{i,j-2} + \alpha 5 \left(\frac{\partial \Psi}{\partial y} \right)_{i,j} \quad \text{(FF9)}$$

We then substitute in the necessary Taylor expansion of Ψ in order to get ω in terms of $\frac{\partial \Psi}{\partial x}$, $\frac{\partial \Psi}{\partial y}$, $\frac{\partial^2 \Psi}{\partial x^2}$, $\frac{\partial^2 \Psi}{\partial y^2}$ and $\Psi_{i,j}$. After factoring the α's and equating it to Equation FF1, we get:

$$-\left(\frac{\partial^2\Psi}{\partial x^2}+\frac{\partial^2\Psi}{\partial y^2}\right)=(\alpha_1+\alpha_2+\alpha_3+\alpha_4+\alpha_5)\Psi_{i,j}+\frac{\partial\Psi}{\partial x}(-\alpha_3+\alpha_4)dx+\frac{\partial\Psi}{\partial y}((\alpha_1+2\alpha_2+\alpha_3+\alpha_4)dy+\alpha_5)+\frac{\partial^2\Psi}{\partial y^2}($$ (FF10)

By equating similar terms from the right and left side of Equation FF10, we can define a linear system of five equations that can be used to solve for the unknown α's. As an example, one such equation is the coefficients of $\Psi_{i,j}$ on the right side will be equal to 0 since there is no $\Psi_{i,j}$ term on the left. Using the five equations generated this way, we solve for the values of α and use them to define the boundary conditions for ω.

The vorticity can be a function that is made very general, or one that is very specific. First, we used a general case to model fluid flow, which was not specific to our system. The equation for ω in a general fluid flow model is shown in Equation FF11.

$$\nabla^2\omega=0=\frac{\partial^2\omega}{\partial x^2}+\frac{\partial^2\omega}{\partial y^2}$$ (FF11)

After using this definition of vorticity and validating the results of the stream function for a general system, a different and more accurate definition of vorticity was used. As defined in Equation FF12, this definition of ω takes into account system-specific parameters such as viscosity, characteristic length, etc. This equation was adapted from [16].

$$U\frac{\partial\omega}{\partial x}+V\frac{\partial\omega}{\partial y}=\frac{\varepsilon}{Re}\left(\frac{\partial^2\omega}{\partial x^2}+\frac{\partial^2\omega}{\partial y^2}\right)-\frac{\varepsilon^2}{DaRe}\omega-\frac{F\varepsilon^2}{\sqrt{Da}}\|\mathrm{v}\|\omega$$ (FF12)

where U and V are dimensionless interstitial velocity components in the x and y directions, respectively, and ||v|| is the magnitude of the interstitial velocity vector. In addition, ε is the porosity of the medium, *Re* is the Reynolds number, *Da* is the Darcy number, and F is a geometric function. The porosity of our porous graphene was calculated to be 85.5% [1]. Using the definition of F, the value of the geometric function is shown below [16].

$$F=\frac{1.75}{\sqrt{150\varepsilon^3}}\approx.018$$ (FF13)

The Reynolds number was calculated using estimated values from literature and material specifications. The definition and approximate value is shown below.

$$Re=\frac{\rho v_{oil}H}{\mu}\approx1.7\cdot10^{-5}$$ (FF14)

where ρ is the density of the fluid, v_{oil} is the mean velocity of the oil and determined experimentally, H is the characteristic length dimension, and μ is the dynamic viscosity. The estimation for the Darcy number is similarly shown below.

$$Da=\frac{K}{H^2}\approx3\cdot10^{-9}$$ (FF15)

where K is the permeability of the porous graphene and H, again, is the characteristic length dimension. Finally, the dimensionless interstitial velocity components are defined by the stream function as shown below.

$$U=\frac{\partial\Psi}{\partial x}\text{ and }V=\frac{\partial\Psi}{\partial y}$$ (FF16,FF17)

Since the stream function and vorticity are defined as a function of both themselves and the other function, an implicit solution was used to solve Equation FF1. Using an initially empty matrix that is filled with each iteration, Equation FF1 was iteratively solved until the stream function and vorticity both converged to an error of less than 0.0001% between successive iterations.

Key assumptions in this model include the assumption that the pores are uniformly distributed throughout the material and the porosity in the x-direction is equal to the porosity in the y-direction. The former is justified by [1]. Although we acknowledge that the x and y porosities vary, the sheet structure of the porous graphene make the effective porosity similar enough for the simulation, considering the limited flow in the x direction. In addition, we are assuming the influence of gravity is negligible. Finally, we have made the assumption that the system is initially empty due to the complexity of the simulation, which will be important while analyzing results.

Once the simulation reaches steady state, we display the stream function matrix as a colormap and a contour plot (Figure 10). In the case where the graphene sponge has only one side exposed to the oil (as processed), it can be noted that steady state is achieved and there is not fluid flow deep into the porous graphene.

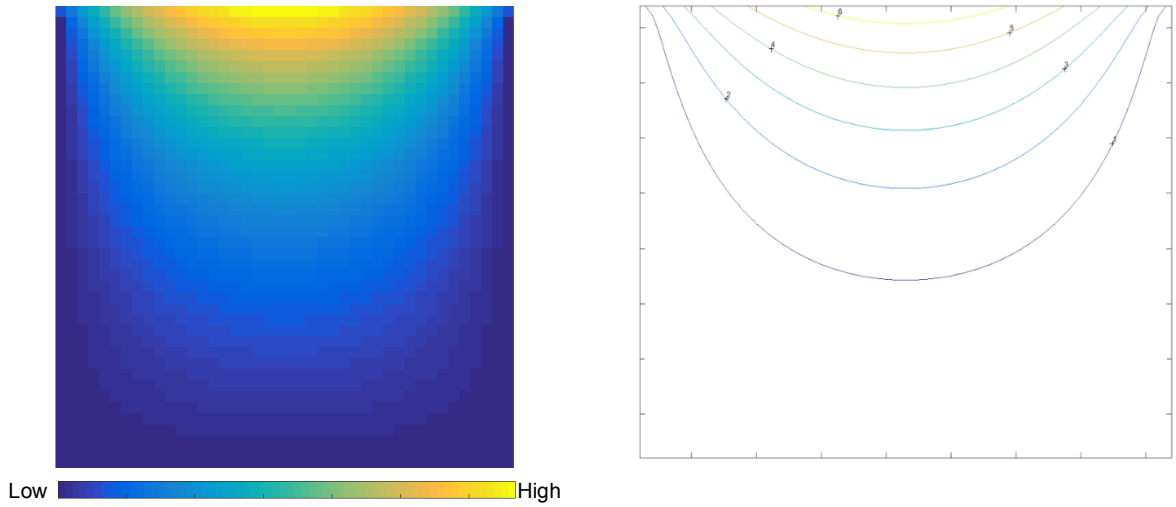

Figure 10. Colormap and contour plot for stream function matrix at steady state.

Using Equations FF16 and FF17, vector plots of the fluid flow velocity can be generated. In the case of the system that is closed on each side, the velocity vector plot is shown in Figure 11.

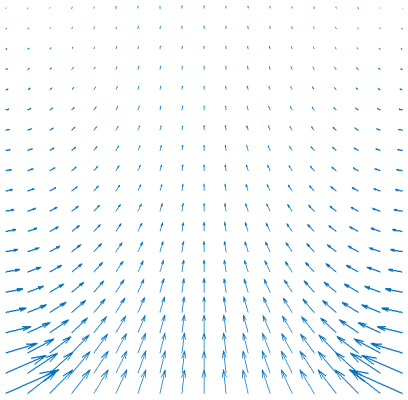

Figure 11. Velocity vector plot of fluid flow.

As apparent, the fluid is flowing into the sample through the barrier between the oil and the porous graphene, but not through the PI. It is also apparent that the fluid flow quickly approaches zero (shorter vectors) as the fluid progresses into the graphene. It is at this point that the assumptions play a key role. Since the initial conditions establish a zero matrix, or empty porous graphene, the fluid flows in readily. But, as evident by the lack of flow out of the porous graphene system, air cannot escape. As a simple analogy, this concept is similar to what occurs when placing an empty glass in water completely upside down and seeing that the water does not fill the glass. The air becomes trapped in our porous graphene sponge, because the fluid flow velocity vectors show a pressure being distributed over the entire opening of the graphene. So, the closed system as in Figure 9, will not uptake any oil.

One of the benefits of this simulation is being able to test various boundary conditions and structures of the porous graphene and PI structure that we may not be able to fabricate currently. So, to mitigate the problem of air being trapped, we implemented macroscopic pores in the PI. To this, we altered the boundary conditions of CD in Figure 3b. Specifically, rather than setting $\frac{\partial \Psi}{\partial y} = 0$, we calculated the proper velocity to maintain mass balance and steady-state diffusion. Effectively, the oil is being removed at the same rate that it is being added. The color map of this situation, with a porous PI substrate is shown in Figure 12. Specifically, we incorporated three openings in the bottom sheet uniformly distributed over the back area. It can be seen that the new openings help fill the nodes more efficiently. The vector map for this situation is shown in Figure 13.

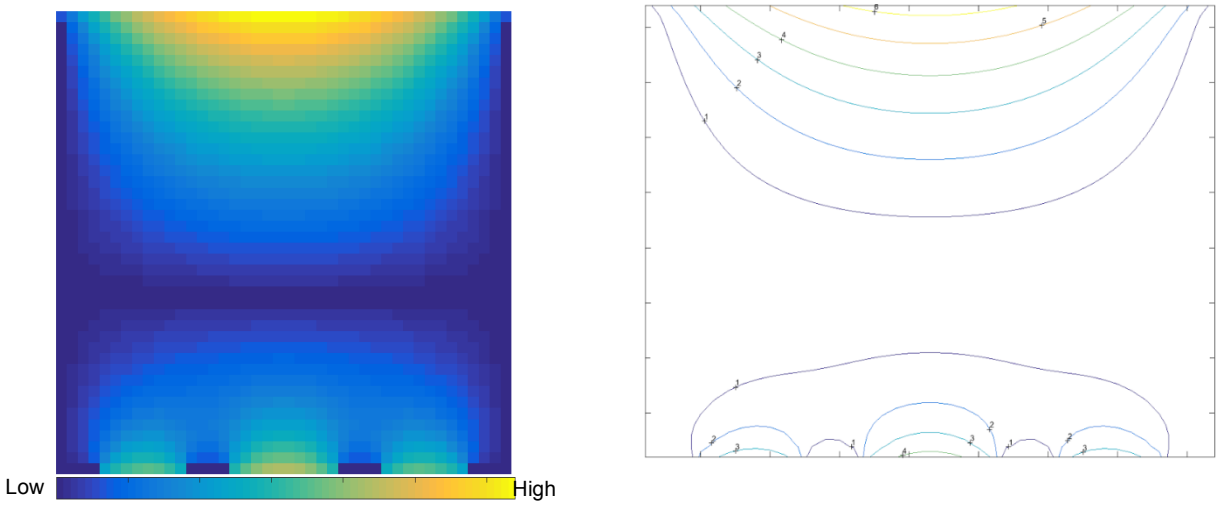

Figure 12. Colormap and contour plot of a system with open pore ventilation on the bottom side.

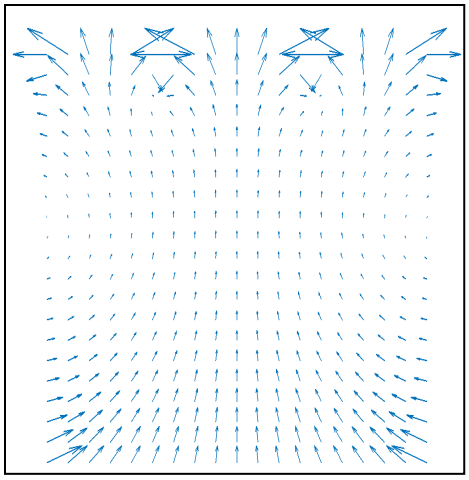

Figure 13. Vector map corresponding to the system with back sheet pore (Figure 12).

The increased overall velocity of fluid from Figure 13 compared to Figure x11 is excellent for a sponge. Primarily, the uptake time be significantly reduced, meaning there will be less time required to reach maximum absorption. Additionally, unlike Figure 11, Figure 13 will allow the fluid to reach all internal areas of the porous graphene, according to our model and solely considering macroscopic flow. So, if the oil molecules truly adsorb to the surface of the graphene sheets, the sorption will be significantly higher with the back open.

Finally, we modelled the fluid flow after completely opening the bottom side, which should be the optimal design for high velocity fluid flow. The colormap and contour of the stream function in this design are shown in Figure 14 while the velocity vector map is shown in Figure 15. The vertical symmetry in Figure 14 is expected, because the openings on either side are exactly the same. The uniformity of the vector arrows in Figure 15 show that the air (initially) and then any fluid that exits the sponge can flow through the sponge with very little impedance. As before, this means considering Darcy's Law only, the uptake will occur more rapidly and there will be more opportunities for the oil molecules to adsorb on the surface of the graphene.

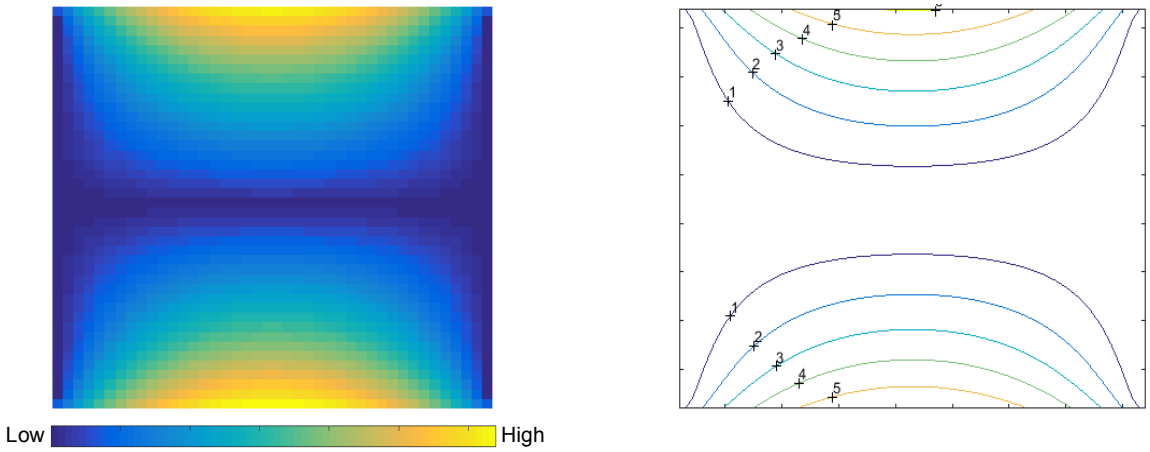

Figure 14. Colormap and contour map of two fully (front,back) opened graphene faces.

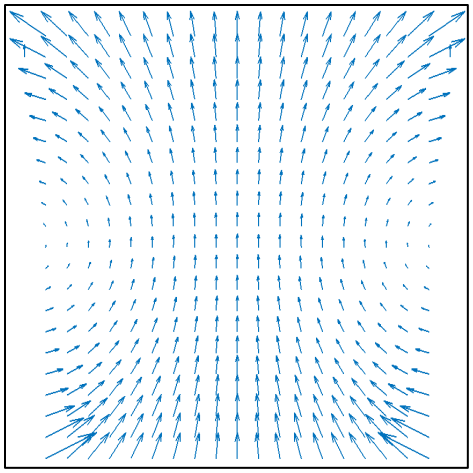

Figure 15. Vector map for system with front and back open graphene faces.

It is important to note that the enhancements realized in these simulations may be ineffective due to nanoscale interactions or factors that were not anticipated. However, this model helps up design an effective sponge from the standpoint of fluid flow and Darcy's Law. In addition, after this model in dimensionalized and validated by experimentation, it can be a powerful tool to elucidate the effect of porosity, fluid viscosity, fluid density, and incident velocity on fluid flow. From the results in this model, we believe opening the reverse side of the PI film (to the air) is essential in designing a more effective sponge for oil sorption.

Experimental

From experimentation, we discovered and documented the quantitative values for grams of oil sorbed per gram graphene of two of our sponges as well as some qualitative sorption related behaviors including capillary action, degradation, selectivity, and evaporation. The quantitative experimentation yielded values for grams oil sorbed per gram graphene much lower than the expected values from literature. As stated before, previous studies on porous graphene and graphite have yielded oil sorptions upwards of 80 grams of oil per gram graphene. Our prototypes absorbed 9.859 mg and 9.816 mg octane with 1.22 and 1.25 mg graphene respectively. Thus, we found the grams oil sorbed per gram of graphene to be approximately 8.08 grams per gram and 7.83 grams per gram for the two samples that were tested and had graphene exfoliated. This is an order of magnitude lower than expected, but we are aware of many methods that can increase the oil sorption, perhaps even dramatically.

We also found, quantitatively, the sorption vs. time through capillary effects of each sample. The linear behavior of capillary sorption, Figure 16a, is indicative of a time dependent sorption. Fully submerging the samples showed instantaneous saturation, Figure 16b, thus decreasing flow velocity to 0 and restricting the oil's movement through the sample. This supports the hypotheses formulated from the fluid flow models regarding the closed system and we believe it was caused by air trapped within the LIG. When a portion of the sponge is exposed to air, the oil displaces air pockets trapped within the sample, thereby supporting the fluid flow model. We therefore conclude from this set of experiments that there is a possibility of increasing oil sorption by opening the device to air on additional faces.

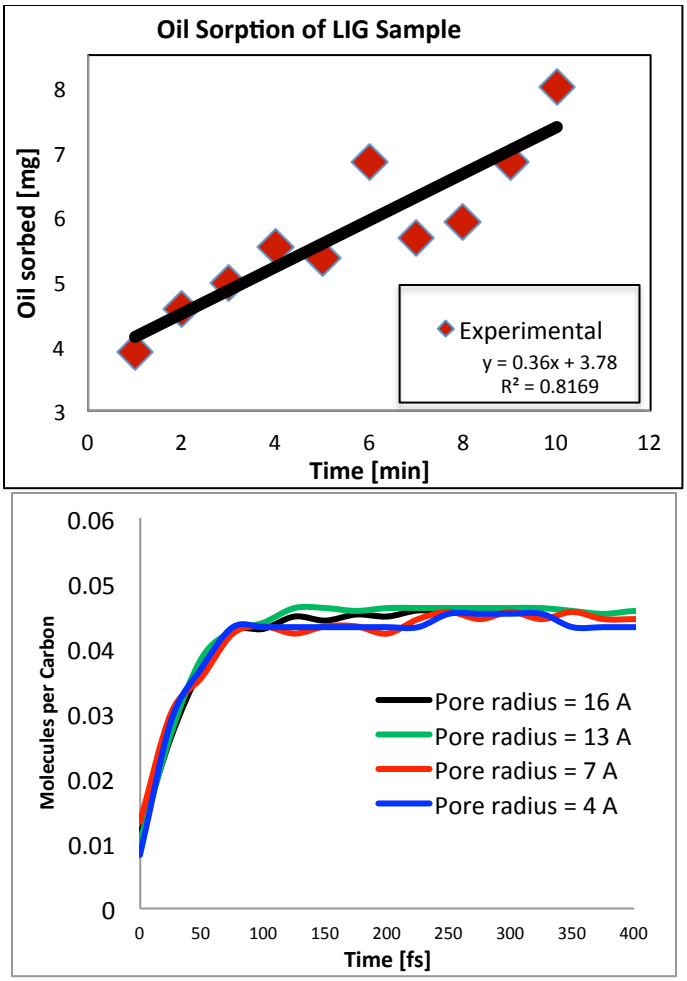

Figure 16. a) Oil sorption as a function of time showing capillary effects. b) instantaneous submersion and oil uptake.

Qualitatively, our experiments demonstrated capillary action, degradation, selectivity and evaporation. We were able to observe capillary action occurring within the sponge. As shown in Figure 17, octane was able to steadily work its way up against gravity to fill the sponge, signifying that the sorption characteristics of the graphene were favorable for alkane sorption. The capillary behavior of octane in graphene asserts sponge-like behavior rather than scooping or skimming behaviors (i.e oil will absorb into the sponge without external guiding forces).

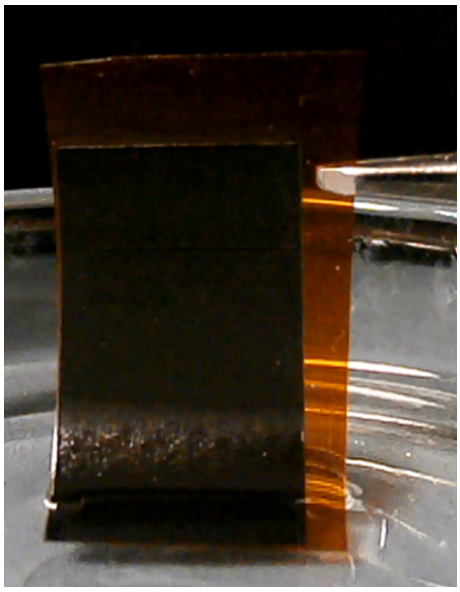

Figure 17. LIG oil sponge partially dipped in octane. The image shows a) the octane level in the dish, b) the uptake of octane by capillary action, c) dry graphene above the uptake line.

We were also able to see flaking of graphene in the octane. This degradation was minimal; however, it does signify that the structural integrity of the device may be called into question. Quantifying the loss was not possible due to the flaked graphene being uncollectable and too small a mass to measure. For future studies, we will attempt to understand material loss and find ways of rectifying any issues that arise due to flaked graphene losses.

Another behavior we were able to successfully document was selectivity, specifically, oleophilicity and hydrophobicity. By conducting a simple drop test, Figure 18, we could see that water would not wet the graphene while octane would. The water droplet beaded up with a wetting angle much larger than 90 degrees. The octane drop did not bead up and simply wetted the graphene. This selectivity is integral to the high sorption efficiency of graphene.

Figure 18. Left: Non-wetting water droplet on LIG oil sponge. Right: Wetted and absorbed octane droplet.

Finally, we observed the quick evaporation of octane. Because of our small sample size and the volatile nature of octane, we observed evaporation of octane from the sample upon removal from the oil bath. This evaporation occurred at about -0.0354mg/s initially, slowing to -0.029mg/s after one minute, and leveling off after 4 minutes, where barely any evaporation occurred. After 5 minutes, the sample was found to be its original weight before submersion, suggesting all octane present evaporated during this time period. While this is an issue for octane and therefore other short chain alkanes, we expect longer

alkanes present in crude oil will not evaporate as quickly due to their lower volatility. This issue does not concern oil removal since the oil is still being removed from the water, but instead concerns recyclability of the oil after removal.

From these simulations and experiments we expect that the most impactful factor contributing to our low sorption is surface absorption. Our simulations support the notion that the octane does not absorb into the spacing between sheets and our experimental data shows much lower sorption than expected. We also expect lower sorption because the device, as seen earlier in this report, is open on a single face which could result in air pocket pressure in the sponge. By partially submerging our sponge, we allowed for the octane to fill our sponge by capillary action. We expect that by using a porous substrate or ablating the entire thickness of the PI film, we would allow for more air and oil to flow through the sponge, increasing sorption.

Conclusions and Future Work

The results of our project can be summarized in a handful of statements: 1) the LIG oil sponge did not perform up to the experimental standards set by other carbon-based oil sponges in literature, 2) both our atomistic and fluid flow modeling suggest the presence of sorption inhibitors, 3) factors including surface adsorption and nonideal design could have contributed to the lowered oil sorption, and 4) further engineering of our device design opens up opportunities for higher oil sorption.

Compared to other carbon-based sponges (e.g. CNT, graphite foam, etc.), the current LIG oil sponge is not as effective as an oil sorption device. Literature values have been recorded upwards from 70 grams of oil per gram of graphene whereas our sorption values of approximately 8 grams of oil per gram of graphene are an order of magnitude lower. From our experimental data, we concluded that there is a mechanism for sorption inhibition. Atomistic simulation suggest that alkanes are energetically unfavorable in intersheet states; however, our fluid flow models show a promising method of increasing the absorption of oil in our device by opening the back face of the sponge.

With extra time, funding, and resources, we could propagate this research into the future in order to fabricate and study an ideal device – one that has a front and back open face – as well as testing LIG with different pore characteristics. The fluid flow models have led us to believe that increasing the sorption of our device is highly feasibly. We could also use actual crude oil instead of an alkane representation of crude oil. Mechanical stability of the devices should be taken into consideration as well.

Acknowledgements

Dr. S. Ehrman - discussion
Dr. J. Klauda - discussion
Dr. P. Kofinas - laboratory facilities
Dr. D. Liu - discussion
Dr. Y. Mo - discussion
Dr. R. Phanuef - discussion and guidance
Dr. S. Phillpot - discussion
Dr. C. Preston - discussion
Dr. C. Thamire - discussion
Dr. J. Tour - samples
A. Kemp - discussion
S. Lacey - computational resources
K. Rohrbach - discussion
M. Widstrom - laboratory supervision
UMD Deepthought - computational resources
UMD OTC - patent provisional

References

1. Lin, J., et al., *Laser-induced porous graphene films from commercial polymers.* Nat Commun, 2014. **5**.
2. Nomack, M., *Environmental impacts of oil spills*, E.P. Agency, Editor. 2010: The Encylopedia of Earth.
3. Inagaki, M., et al., *Sorption and recovery of heavy oils by using exfoliated graphite Part II: Recovery of heavy oil and recycling of exfoliated graphite.* Desalination, 2000. **128**(3): p. 213-218.
4. Fingas, M., *A Review of Literature Related to Oil Spill Solidifiers 1990-2008*, I.C.C.o.O.P.R. (ICCOPR), Editor. 2008, Spill Science: Edmonton, Alberta.
5. Zhou, M.H. and W.-J. Cho, *Oil absorbents based on styrene–butadiene rubber.* Journal of Applied Polymer Science, 2003. **89**(7): p. 1818-1824.
6. Zhou, X., et al., *Facile Fabrication of Superhydrophobic Sponge with Selective Absorption and Collection of Oil from Water.* Industrial & Engineering Chemistry Research, 2013. **52**(27): p. 9411-9416.
7. Hashim, D.P., et al., *Covalently bonded three-dimensional carbon nanotube solids via boron induced nanojunctions.* Sci. Rep., 2012. **2**.
8. BP. *BP Assurance: Independent Assurance Statement to BP Management*. 2015.
9. Bi, H., et al., *Spongy Graphene as a Highly Efficient and Recyclable Sorbent for Oils and Organic Solvents.* Advanced Functional Materials, 2012. **22**(21): p. 4421-4425.
10. Maldonado, E., M. Roth, and P.A. Gray, *Fully Atomistic Molecular Dynamics Simulations of the Behavior of a Simple Model of Crude Oil Confined between Graphene Planes.* ACS applied materials & interfaces, 2009. **1**(6): p. 1211-1217.
11. Whitaker, S., *Flow in porous media I: A theoretical derivation of Darcy's law.* Transport in Porous Media, 1986. **1**(1): p. 3-25.
12. DeMaria, A.J. and J. Thomas V. Hennessey, *CO2 Laser*, in *SPIE Professional*. 2010.
13. Qualters, C., et al., *Carbon Aerogels for Thermal Clothing Applications.* 2015.
14. Kamiya, K. and S. Okada, *Energetics and Electronic Structures of Alkanes and Polyethylene Adsorbed on Graphene.* Japanese Journal of Applied Physics, 2013. **52**(6S): p. 06GD10.

15. Lee, G.-D., et al., *Vacancy defects and the formation of local haeckelite structures in graphene from tight-binding molecular dynamics.* Physical Review B, 2006. **74**(24): p. 245411.
16. Al-Amiri, A.M., *Analysis of momentum and energy transfer in a lid-driven cavity filled with a porous medium.* International Journal of Heat and Mass Transfer, 2000. **43**(19): p. 3513-3527.